PHYSICAL REVIEW D **88,** 025038 (2013)

Holographic pomeron and entropy

Alexander Stoffers and Ismail Zahed

Department of Physics and Astronomy, Stony Brook University, Stony Brook, New York 11794-3800, USA

(Received 30 November 2012; revised manuscript received 30 May 2013; published 22 July 2013)

In dipole-dipole scattering at large rapidity $\chi = \ln(s/s_0)$, the induced instanton on the string world sheet carries entropy $\mathbf{S}_k = 2(\alpha_{\mathbf{P}k} - 1)\chi$, with $\alpha_{\mathbf{P}k} - 1$ the Pomeron intercept for a dipole source of N-ality k. We argue that this entropy is released promptly over a time $t_R \approx (\mathbf{b}_\perp/\chi)^3/(4\alpha')$, with $\alpha'/2$ the Pomeron slope and $\mathbf{b}_\perp$ the impact parameter. This stringy entropy may explain the $3/2$ jump in the total charged multiplicities at about ten participants reported over a wide range of collider energies by PHOBOS. We predict the charged multiplicities in pp, pA and central AA collisions at LHC.

DOI: 10.1103/PhysRevD.88.025038 PACS numbers: 11.80.−m, 11.25.Tq, 25.75.−q

I. INTRODUCTION

The issue of how entropy is released in hadron-hadron and nucleus-nucleus collisions is a fundamental problem in the current heavy-ion program at collider energies. How coherence, which is a hallmark of a fundamental collision, turns to incoherence, which is at the origin of the concept of entropy, is a theoretical question of central importance. A possible understanding for the entropy deposition was attempted at weak coupling through the concept of the color glass approach in classical but perturbative QCD [1–3] and at strong coupling through the concept of black hole formation in holographic QCD [4–8].

The evidence of a strongly coupled plasma released at collider energies, with large and prompt entropy deposition and flow, suggests that a strong coupling approach is needed for the mechanism of entropy decomposition. In this way, the holographic approach with the release of a black hole falling along the holographic direction provides a plausible mechanism for entropy production. However, this mechanism is detached from our understanding of fundamental pp collisions, which are, after all, the seeds at the origin of the entropy production. This paper is an attempt to provide such an understanding.

pp collisions at large rapidity are dominated by Pomeron and Reggeon exchange [9,10]. In the kinematic region $\sqrt{s} \gg \sqrt{-t}$, Pomeron exchange dominates the eikonalized scattering amplitude, which is modeled though gluon ladders at weak coupling [11]. At large N_c and strong coupling, the Pomeron exchange has a simple holographic realization as noncritical closed-string exchange in the t channel in $D = 5$ [12]. For early approaches, see Refs. [13,14]. For a description of the Pomeron as a closed-string exchange in critical $D = 10$ dimensions using the Virasoro-Shapiro string amplitude, see Ref. [15].

At large rapidity χ, this string exchange is characterized by an effective Unruh temperature, which is set by the impact parameter and the collision energy. This temperature emerges from a longitudinal acceleration of the string caused by a global and longitudinal "electric field" on the string world sheet. This global electric field encodes twisted boundary conditions and gives rise to a stringy instanton as the Pomeron in dipole-dipole scattering at large rapidity. Below, we suggest that the Unruh temperature causes the string to partially vibrate and thus carry entropy. The idea of relating the Hawking-Unruh radiation of a black hole to radiative processes in a color-confining theory such as QCD was explored in Ref. [16] using different arguments.

In Secs. II and III, we recall the holographic dipole-dipole scattering formulation through bosonic string exchange [12] and the close connection to Gribov diffusion in curved space [17]. In Sec. IV, we revisit the arguments for the emergence of a stringy instanton presented in dipole-dipole scattering. We then review the connection between the Schwinger pair-production formalism and the Unruh effect in Sec. V to obtain the entropy released in the collision in Sec. VI. We derive the entropy associated with the stringy instanton and tie it with the wee-dipole multiplicity characteristic of the one-Pomeron exchange. We further estimate the time it takes for this entropy to be deposited in Sec. VII. In Secs. VIII and IX, we suggest that this stringy entropy is at work in pp, pA and AA collisions at collider energies and show that it can account for a key jump in the total charged multiplicities versus the number of participants as reported by the PHOBOS Collaboration. The obtained charged multiplicities are compared to the pp and AuAu data. We predict the multiplicities for pPb and PbPb at the LHC. Our conclusions follow in Sec. X.

II. HOLOGRAPHIC DIPOLE-DIPOLE SCATTERING

To make our discussion self-contained, we briefly review the basic formulation for the elastic dipole-dipole scattering amplitude through a Wilson loop correlator [18–21] and its holographic translation [12]. Each dipole is described by a Wilson loop, and we seek to express the scattering amplitude in terms of the two-loop correlator. The kinematics is captured by a fixed impact parameter $\mathbf{b}_\perp$, conjugate to the transferred momentum $\mathbf{q}_\perp$, and the

rapidity interval χ related to the collisional energy. At high energies, the T matrix factorizes [19,22,23]:

$$\mathcal{T}_{12\to34}(s,t) = 2is\int du_1 du_2 \psi_4(u_1)\psi_3(u_1) \times \mathcal{T}_{DD}(\chi, \mathbf{b}_\perp, u_1, u_2)\psi_2(u_2)\psi_1(u_2), \quad (1)$$

where u_i is related to the transverse size of the dipole element described by the wave function ψ_i. The dipole-dipole scattering amplitude is given by

$$\mathcal{T}_{DD}(\chi, \mathbf{b}_\perp, u_1, u_2) = \int d^{D_\perp}\mathbf{b}_\perp e^{i\mathbf{q}_\perp\cdot\mathbf{b}_\perp}(1 - \langle \mathbf{W}(C_1)\mathbf{W}(C_2)\rangle_G) \equiv \int d^{D_\perp}\mathbf{b}_\perp e^{i\mathbf{q}_\perp\cdot\mathbf{b}_\perp}\mathbf{WW}, \quad (2)$$

where the integration is taken over the $D_\perp$ dimensional impact parameter space separating the two dipoles. We will use the normalization $\langle \mathbf{W}\rangle = 1$ and focus only on the connected part of the correlator. The subscript G in Eq. (2) indicates that the expectation value of the Wilson loop correlator is taken over gauge fields. This implies that the gluonic flux tube does not brake by dynamic quark-antiquark pair production. At high energies, Pomerons (correlated gluon ladders) dominate over Reggeons (correlated quark-antiquark exchange). The Wilson loops are evaluated along the surfaces C_1, C_2 pictured in Fig. 1. Note that in the eikonal approximation, the ultrarelativistic dipole is a scalar, since it nearly moves on the light cone. In Eq. (2) we have suppressed a dependence on the individual momenta of the dipole constituents and assumed that the total momentum of each dipole is equally distributed between its constituents. The effective size of the dipole is at a maximum when the momentum is unequally distributed, and hence, we are restricting our analysis to small dipoles.

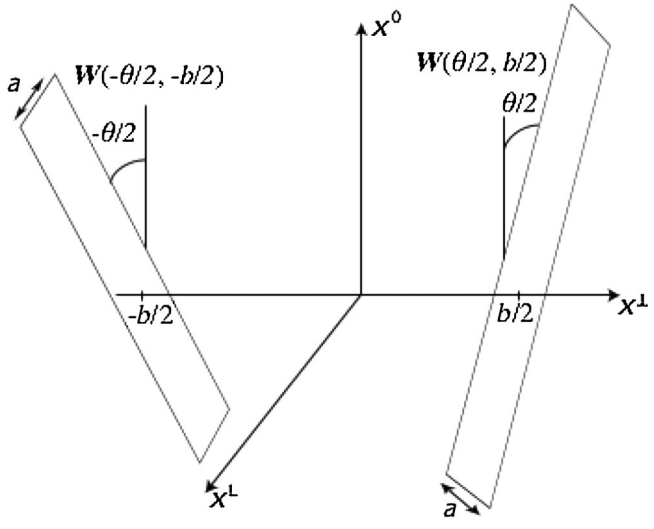

FIG. 1. Dipole-dipole scattering in Euclidean space; see text. Reprinted with permission from G. Basar *et al.*, Phys. Rev. D 85, 105005 (2012). Copyright 2012, American Physical Society.

Early calculations of the Wilson loop correlator in a static setup are found in Refs. [24–26]. The correlator between two circular loops is stable when the distance separating the loops is of the order of the radius of the individual loops. A Gross-Ooguri phase transition [25] occurs when this distance is much larger than the radius; in order to elongate the surface in bulk, supergravity interactions in bulk between the two lumps are needed. In a non-supersymmetric setup, the potential between two heavy mesons is generated by the exchange of a "scalarball" [27].

In order to access the scattering amplitude, the boundary conditions for the Wilson loops change from a static to a *dynamic setup*. In Euclidean space, this amounts to changing the angle θ to a nonzero value. This is illustrated in Fig. 1. The role of the angle is played by the rapidity interval after analytic continuation. This will generate a tunneling contribution absent in the potential. This tunneling contribution will be at the origin of the entropy in the elastic scattering amplitude, as we detail below. This is one of the fundamental observations of this paper.

The problem of finding a minimal surface to the dynamic setup in Fig. 1 has a long history. Early approaches [13] attempting to solve for a string world sheet at constant time slices yield a Reggeized amplitude at large s, but fail to describe inelastic processes and give a negative Pomeron intercept. In Ref. [14], a first-order perturbation in the bulk AdS fields is taken into account. The intercept is purely kinematical, i.e. equal to 1 for the case of the graviton, as compared to the QCD expectation $s^{4/\pi\alpha_s N_c \ln(2)}$.

When the dipoles are small compared to the impact parameter and the rapidity interval is large, the surface connecting the two dipoles is highly twisted and can be approximated by the world sheet of a string with the appropriate boundary conditions; see Fig. 2. In general, the surface is exchanged in $D_\perp$ dimensions. Below, we show that a detailed comparison with QCD BFKL expectations and experimental data suggests $D_\perp = 3$ [17,28]. The curved holographic coordinate scales the momenta of the dipoles [29]. Accordingly, the change in the curved holographic coordinate, or z, from one end of the string to the other is proportional to the momentum transfer between the dipoles. Thus, in the Regge regime with $\sqrt{s} \gg \sqrt{-t} = \mathbf{q}_\perp$, the string is exchanged in an approximately flat background for a confining metric. To describe a scattering process in which a colorless object is exchanged, the string is bosonic and closed. We will neglect corrections to the tree-level approximation, as the string coupling will be assumed to be small. However, we will not limit ourselves to a classical string configuration but will take into account (quantum) oscillations. A similar idea was put forward more than three decades ago [30].

The problem is set up in Euclidean space and then continued to Minkowski space. Due to the expected pole

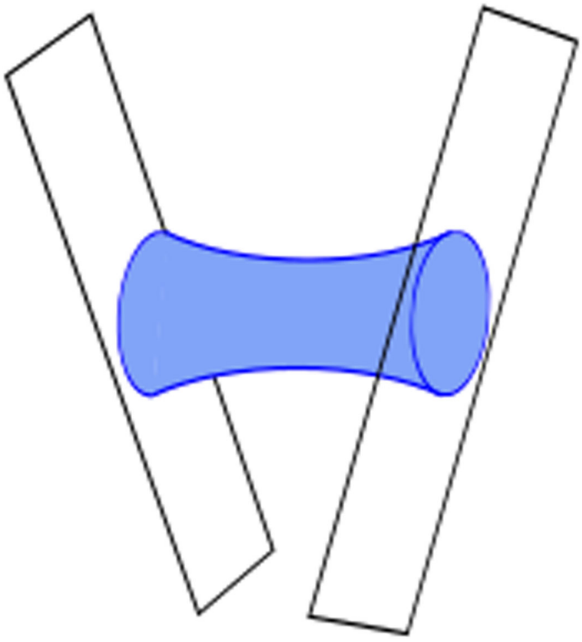

FIG. 2 (color online). Twisted surface connecting the Wilson loops; see text. Reprinted with permission from G. Basar *et al.*, Phys. Rev. D 85, 105005 (2012). Copyright 2012, American Physical Society.

structure of the amplitude, the analytic continuation is by no means trivial. The reliance of the continuation has been tested on the lattice [31,32]. After analytic continuation from Euclidean to Minkowski space, the angle θ is transformed to the rapidity interval $\chi \equiv \chi_{\max} + \chi_{\min} = i\theta$, which is defined by

$$\cos\theta \to \cosh\chi \equiv \frac{1}{\sqrt{1-v^2}} = \frac{s}{s_0} - 1, \tag{3}$$

where the parameter s_0 is related to the effective transverse scattering mass as $s_0 = m_\perp^2 = m^2 + p_\perp^2$.

With $D_\perp = 3$, we will use AdS_5 with an IR cutoff realized through a hard wall at z_0 as a confining background. Although the field theory corresponding to this space is not exactly QCD, it captures some of its essential features [33]. The Euclidean AdS_5 space-time metric is

$$ds^2 = \frac{1}{z^2}((dx^0)^2 + (dx^1)^2 + (dx_\perp^2) + (dz)^2), \tag{4}$$

where we have set the AdS radius to 1. The IR cutoff is at some z_0, i.e. $0 \le z \le z_0$. The dipoles of fixed size a, a' are initially located at the boundary $z \approx 0$. Later, they will be moved to the bulk to account for their varying sizes.

We will now recall the dipole-dipole correlator for small momentum transfer where the background space-time is taken to be *flat* as detailed in Ref. [12] for completeness. In this approximation, the Wilson loop correlator reads

$$\mathbf{WW} = g_s^2 \int_0^\infty \frac{dT}{2T}\mathbf{K}(T). \tag{5}$$

The closed string is parametrized by one parameter, the modulus ("circumference") T. The factor g_s^2 in Eq. (5) comes from the genus of the string configuration compared to the disconnected configuration. The string propagator reads

$$\mathbf{K}(T) = \int_T d[x] e^{-S[x]+\text{ghosts}}. \tag{6}$$

For closed, long strings where the interaction between the strings is negligible, the effective string action is the Polyakov action

$$S = \frac{\sigma_T}{2}\int_0^T d\tau \int_0^1 d\sigma\,(\dot{x}^\mu \dot{x}_\mu + x'^\mu x'_\mu), \tag{7}$$

with $\dot{x} = \partial_\tau x$ and $x' = \partial_\sigma x$. The string tension is $\sigma_T = 1/(2\pi\alpha')$. The Regge slope α' is related to the fundamental string length by $\alpha' = l_s^2$. We have made the following gauge choice for the world-sheet metric: $h_b^a = \delta_b^a$.

The string coordinate $x^\mu(\tau, \sigma)$ is closed,

$$x^\mu(T, \sigma) = x^\mu(0, \sigma), \tag{8}$$

and attaches to the twisted dipole surfaces

$$\cos(\theta/2)x^1(\tau, 0) + \sin(\theta/2)x^0(\tau, 0) = 0, \tag{9}$$

$$\cos(\theta/2)x^1(\tau, 1) - \sin(\theta/2)x^0(\tau, 1) = 0. \tag{10}$$

We already see that the freedom in moving the intersection point of the string world-sheet with the dipole surfaces of width a, a' yields a factor aa' in the correlator [Eqs. (5) and (6)].

The world-sheet is twisted in the x^0, x^1 coordinates

$$\begin{pmatrix} x^0 \\ x^1 \end{pmatrix} = \begin{pmatrix} \cos\theta_\sigma & -\sin\theta_\sigma \\ \sin\theta_\sigma & \cos\theta_\sigma \end{pmatrix}\begin{pmatrix} \tilde{x}^0 \\ \tilde{x}^1 \end{pmatrix}, \tag{11}$$

with $\theta_\sigma = \theta(2\sigma - 1)$. This twist (rotation) in Euclidean space corresponds to a Lorentz boost in the longitudinal direction after analytic continuation.

We can now evaluate the Wilson loop correlator by solving for the bosonic string world-sheet with Neumann boundary conditions for $\tilde{x}^0$ and Dirichlet boundary conditions for $\tilde{x}^1$. The Polyakov action is quadratic in the untwisted coordinates, and the solutions can be parametrized as

$$\tilde{x}^0(\tau, \sigma) = \sum_{m=-\infty}^{+\infty}\sum_{n=0}^{+\infty} x_{mn}^0 e^{2\pi i m\tau/T}\cos(\pi n\sigma), \tag{12}$$

$$\tilde{x}^1(\tau, \sigma) = \sum_{m=-\infty}^{+\infty}\sum_{n=0}^{+\infty} x_{mn}^1 e^{2\pi i m\tau/T}\sin(\pi n\sigma). \tag{13}$$

Note that the temporal component has a nonvanishing ground state similar to a zero mode:

$$\tilde{x}^0_{ZM}(\tau,\sigma) \equiv \sum_{m=-\infty}^{+\infty} x^0_{m0} e^{2\pi i m\tau/T}. \tag{14}$$

The transverse, untwisted coordinates are periodic with Dirichlet boundary conditions

$$x^\perp(\tau,\sigma) = -\mathbf{b}_\perp(1-2\sigma)/2 + \sum_{m=-\infty}^{+\infty}\sum_{n=0}^{+\infty} x^\perp_{mn} e^{2\pi i m\tau/T}\sin(\pi n\sigma). \tag{15}$$

Since the action is quadratic, the propagator [Eq. (6)] factorizes as

$$\mathbf{K} = \mathbf{K}_{0L}\times\mathbf{K}_{\not 0 L}\times\mathbf{K}_\perp\times\mathbf{K}_{\rm ghost}, \tag{16}$$

with the individual contributions $\mathbf{K}_{0L}$, $\mathbf{K}_{\not 0 L}$ from the longitudinal zero/nonzero modes and $\mathbf{K}_\perp$ as the contribution from the $\perp$ modes. Due to the gauge choice for the string world-sheet metric, the propagator gets the ghost contribution $\mathbf{K}_{\rm ghost}$.

The contributions from the longitudinal modes read [12]

$$\mathbf{K}_{0L}(T) = (2\sinh(\theta T/2))^{-1} \tag{17}$$

and

$$\mathbf{K}_{\not 0 L}(T) = \prod_{n=1}^{\infty}\prod_{s=\pm 1}(2\sinh((n+s\theta/\pi)\pi T/2))^{-1}. \tag{18}$$

The transverse part of the propagator is given by

$$\mathbf{K}_\perp = e^{-\sigma_T \mathbf{b}_\perp^2 T/2}\eta^{-D_\perp}(iT/2), \tag{19}$$

with the Dedekind eta function

$$\eta(\tau) \equiv q^{1/24}\prod_n (1-q^n) \tag{20}$$

and $q \equiv e^{2\pi i\tau}$. The ghost contribution to the propagator is given by

$$\mathbf{K}_{\rm ghost}(T) = \prod_{n=1}^{\infty} 4\sinh^2(n\pi T/2). \tag{21}$$

We can now analytically continue from Euclidean to Minkowski space by letting $\theta \to -i\chi$. The loop-loop correlator then reads

$$\mathbf{WW} = g_s^2\int_0^\infty \frac{dT}{2T}\mathbf{K}(T) \tag{22}$$

$$= \frac{ig_s^2 aa'}{4\alpha'}\int_0^\infty \frac{dT}{T}\frac{1}{\sin(\chi T/2)} \times\prod_{n=1}^{\infty}\prod_{s=\pm 1}\frac{\sinh(n\pi T/2)}{\sinh((n\pi+is\chi)T/2)}\eta^{-D_\perp}(iT/2) \times e^{-\mathbf{b}_\perp^2 T/4\pi\alpha'}. \tag{23}$$

For $\chi\to\infty$, we see that the longitudinal zero modes are responsible for the poles along the real T axis. Picking up the residues at the positive poles $T = 2\pi k/\chi$, Eq. (23) equates to

$$\mathbf{WW} = \frac{g_s^2 aa'}{4\alpha'}\sum_{k=1}^{k_{\rm max}}\frac{(-1)^k}{k}\eta^{-D_\perp}(i\pi k/\chi)e^{-k\mathbf{b}_\perp^2/2\alpha'\chi}. \tag{24}$$

Using

$$\eta^{-D_\perp}(i\pi k/\chi) = \left(\frac{\pi k}{\chi}\right)^{D_\perp/2} e^{D_\perp\chi/12k}\prod_{n=1}^{\infty}(1-e^{-2\chi n/k})^{-D_\perp} = \left(\frac{\pi k}{\chi}\right)^{D_\perp/2}\sum_{n=0}^{\infty} d(n)e^{-2\chi n/k}, \tag{25}$$

we can rewrite the Wilson loop correlator as

$$\mathbf{WW} = \frac{g_s^2 aa'}{4\alpha'}\sum_{k=1}^{k_{\rm max}}\sum_{n=0}^{\infty}\frac{(-1)^k}{k}\left(\frac{\pi k}{\chi}\right)^{D_\perp/2} \times d(n)e^{-k\mathbf{b}_\perp^2/2\alpha'\chi + D_\perp/12k - 2\chi n/k}. \tag{26}$$

For large n, the density of string state $d(n)$ rises exponentially [34]:

$$d(n) \sim \frac{e^{2\pi\sqrt{D_\perp n/6}}}{n^{D_\perp/4}}. \tag{27}$$

The correlator [Eq. (26)] is dominated by the lowest transverse mode, $n = 0$. The poles are at different winding k, which is interpreted as the N-ality. For QCD with $N_c = 3$, the exchange is limited to $k = 1, 2$ strings.

III. GRIBOV DIFFUSION IN CURVED SPACE

Gribov diffusion [35,36] is a way to reconcile the partonic picture with the nonperturbative aspects of hadronic interactions at high energies. The assumption is that hadronic interactions at strong coupling are the result of parton emission. Each emission changes the rapidity of the emitting parton, which results in a diffusive motion for the partons in impact parameter space. The difference in rapidities at the initial and following points in space mimics the diffusion in time. The spread in impact parameter space results in a spread in momenta. The higher the energies, the broader the diffusive regime, and lower momenta start to become important. At large momentum, the hadron is Lorentz contracted, and its effective volume grows with $\ln(s)$ [28], while the number of partons scales with the momentum as $s^{\#}$; compare Eq. (40). At higher and higher energies, the wave functions of the partons overlap, and the probability to recombine balances the production. The scattering objects become "black disks." Gribov anticipated that this should result in a constant total cross section for *all* hadronic interactions.

We will now recall that the string exchange picture naturally leads to a diffusive process reminiscent of Gribov diffusion in which the long string diffuses in rapidity through the impact parameter space [17]. The diffusion

constant is related to the 't Hooft coupling λ, and the curvature of the embedding space-time gives a correction to the Pomeron intercept. We will then derive the wee-dipole density and show that it compares to the QCD BFKL expectations, albeit with a nonperturbative intercept and diffusion constant.

Here we note the alternative nonperturbative derivation of the Pomeron as a graviton exchange in ten dimensions discussed in Ref. [15]. While our string exchange and the graviton exchanges as models of the Pomeron are similar in spirit, they are different in content. Indeed, in conformal AdS, multigraviton exchanges are the dominant exchange between small dipoles, while in confined AdS, gravitons are massive on the confinement scale. The interaction between small dipoles is dominated by the exchange of correlated gluons (perhaps fishnets [37]) in the form of a noncritical string exchange. In the conformal limit, both approaches are similar, although with different Pomeron parameters, as thoroughly discussed in Ref. [17].

The Wilson loop correlator [Eq. (26)], and hence the scattering amplitude, is dominated by the tachyonic $n = 0$ contribution. We identify this $n = 0$ mode with the exchanged Pomeron. Specifically, we can rewrite Eq. (24) as

$$\mathbf{WW} \approx \frac{g_s^2}{4}\left(\frac{\pi}{\sigma_T}\right)^{D_\perp/2}\sum_{k=1}^{k_{\max}}\frac{(-1)^k}{k}\frac{aa'}{\alpha'}\mathbf{K}_k(\chi, \mathbf{b}_\perp). \tag{28}$$

The emerging propagator at the poles,

$$\mathbf{K}_k(\chi, \mathbf{b}_\perp) = \left(\frac{k}{2\pi\alpha'\chi}\right)^{D_\perp/2} e^{-k\mathbf{b}_\perp^2/2\chi\alpha' + D_\perp\chi/12k}, \tag{29}$$

satisfies a diffusion equation in flat space,

$$(\partial_{T_\perp} + (M_0^2 - \nabla_\perp^2))\mathbf{K}_k(T_\perp, M, \mathbf{b}_\perp) = 0, \tag{30}$$

after the identification of the proper time $T_\perp = \mathbf{D}_k\chi$ with the diffusion constant $\mathbf{D}_k = \alpha'/2k$. The tachyonic mass follows from the harmonic string spectrum

$$M_n^2 = \frac{4}{\alpha'}\left(n - \frac{D_\perp}{24}\right) \to -\frac{D_\perp}{6\alpha'}. \tag{31}$$

While the tachyon is a nuisance for the string potential problem, which is overcome by dialing the string in critical dimensions, it is an asset for the dipole scattering problem in any dimension, as it translates to the Pomeron intercept.

Assuming that, for short proper times, $T \sim 1/\chi < 1$, the longitudinal pole structure of the diffusion kernel is unchanged, the tachyonic string receives curvature corrections for transverse modes. These are readily calculated by letting [28]

$$\frac{aa'}{\alpha'}\mathbf{K}_k(\chi, \mathbf{b}_\perp) \to zz'\mathbf{N}(\chi, z, z', \mathbf{b}_\perp). \tag{32}$$

As a result, we identify $\mathbf{N}$ with the wee-dipole density. In a curved background with a confining hard wall, this wee-dipole density $\mathbf{N}$ can be obtained in closed form using the initial condition [$u = -\ln(z/z_0)$],

$$\mathbf{N}(\chi = 0, u, u', \mathbf{b}_\perp) = \delta(u - u')\delta(\mathbf{b}_\perp), \tag{33}$$

and the infrared or wall boundary condition

$$\partial_{u=0}\mathbf{N} = 0 \tag{34}$$

as detailed in Ref. [28]. The explicit solution is

$$\begin{aligned}\mathbf{N}(T_\perp, u, u', \mathbf{b}_\perp) &= \frac{1}{z_0^2}e^{u'+u}\Delta_\perp(\chi, \xi) + \frac{1}{z_0^2}e^{u'-u}\Delta_\perp(\chi, \xi_*)\\ &= \frac{1}{zz'}\Delta_\perp(\chi, \xi) + \frac{z}{z'z_0^2}\Delta_\perp(\chi, \xi_*).\end{aligned} \tag{35}$$

Here $\Delta_\perp$ is the diffusive kernel in curved holographic space without a wall,

$$\left(\partial_{T_\perp} + \left(M_0^2 - \frac{1}{\sqrt{g_\perp}}\partial_\mu g_\perp^{\mu\nu}\sqrt{g_\perp}\partial_\nu\right)\right)\Delta_\perp(x_\perp, x'_\perp) = 0, \tag{36}$$

with a delta-function initial condition. Explicitly,

$$\Delta_\perp(\chi, \xi) = \frac{e^{j_0\mathbf{D}\chi}}{(4\pi\mathbf{D}\chi)^{3/2}}\frac{\xi e^{-\frac{\xi^2}{4\mathbf{D}\chi}}}{\sinh(\xi)}, \tag{37}$$

with the chordal distances

$$\cosh\xi = \cosh(u' - u) + \frac{1}{2}\mathbf{b}_\perp^2 e^{u'+u}, \tag{38}$$

$$\cosh\xi_* = \cosh(u' + u) + \frac{1}{2}\mathbf{b}_\perp^2 e^{u'-u}. \tag{39}$$

The physical interpretation of $\mathbf{N}$ is that of the wee-dipole of scale u at a transverse distance $\mathbf{b}_\perp$, sourced by a dipole of scale u' located at $\mathbf{b}'_\perp = \mathbf{0}$. The wee-dipole cloud is captured by the string at strong coupling. In a way, this is the "Weizsaecker-Williams" dipole cloud as captured by the string sourced by a mother dipole. It normalizes to

$$N_{\text{wee}} = \int du d\mathbf{b}_\perp \mathbf{N} = e^{-T(M_0^2 + D_\perp - 2)} \equiv (s/s_0)^{\alpha_{\mathbf{P}}-1} \tag{40}$$

with the $1/\sqrt{\lambda}$ corrected intercept

$$\alpha_{\mathbf{P}} = 1 + \frac{D_\perp}{12} - \frac{(D_\perp - 1)^2}{8\sqrt{\lambda}}. \tag{41}$$

For $\frac{\mathbf{b}_\perp^2}{2zz'} \gg 1$, the analytic form of this holographic wee-dipole density in $D_\perp = 3$ exactly matches the BFKL result [17]. Perturbative gluon ladders transmute to string world-sheets at strong coupling, a point at the origin of the QCD fishnet approach to large Wilson loops for the potential problem [37]. The ordered BFKL resummation of perturbative QCD diagrams is encoded in the stringy Schwinger mechanism discussed in Ref. [12], albeit in hyperbolic space. Finally, and in terms of Eq. (32), the leading ($k = 1$) contribution to Eq. (5) in a curved AdS background reads

$$\mathbf{WW} \approx -\frac{g_s^2}{4}(2\pi\alpha')^{3/2} zz' \mathbf{N}(\chi, z, z', \mathbf{b}_\perp). \tag{42}$$

IV. STRINGY INSTANTON

We will now briefly explain the factor $e^{-k\mathbf{b}_\perp^2/2\chi\alpha'}$ in the correlator [Eq. (26)], which drives the Regge behavior of the scattering amplitude as detailed in Ref. [12]. The kth contribution comes from the poles, and the pole structure originates from the twist in the longitudinal modes. The rapidity triggers an electric field acting on the end points of the open string. In Euclidean space, this electric field causes tunneling and, therefore, an instanton. In Minkowski space, this instanton captures the pair-creation process of the stringy Schwinger mechanism. Pair creation means inelasticities and entropy.

The instanton is best described by using the T-dual transformation of the string coordinates:

$$\partial_\tau x^1 = \partial_\sigma y^1, \tag{43}$$

$$\partial_\sigma x^1 = \partial_\tau y^1, \tag{44}$$

for which the Polyakov action [Eq. (7)] now reads

$$S = \frac{\sigma_T}{2}\int_0^T d\tau \int_0^1 d\sigma((\partial x^0)^2 + (\partial y^1)^2 + (\partial x^\perp)^2) + \frac{E}{2}\int_0^T d\tau (y^1\partial_\tau x^0 - x^0\partial_\tau y^1)|_{\sigma=0,1}, \tag{45}$$

with

$$E = F_{01} = \sigma_T \tanh(\chi/2). \tag{46}$$

In the T-dual form, the twisted boundary conditions transmute to an electric field [Eq. (46)] along the y^1 direction. This electric field is purely kinematical and is at the origin of the world-sheet instanton as we now detail.

The semiclassical extrema of Eq. (45) can be labeled by $k > 0$. They follow from the saddle points of Eq. (45) along T and the world-sheet coordinates. Explicitly, for $x^\perp = \mathbf{b}_\perp \sigma$,

$$\begin{aligned} x^0 &= R(\sigma)\cos(2\pi k\tau/T), \\ y^1 &= R(\sigma)\sin(2\pi k\tau/T), \end{aligned} \tag{47}$$

with $R(\sigma) = (\mathbf{b}_\perp/\chi)\cosh(\chi(\sigma - 1/2))$. The saddle point of Eq. (45) along the T direction is algebraic, giving $T = 2\pi k/\chi$. A similar world-sheet instanton for D-brane scattering was discussed in Ref. [38]. In the terms of Eq. (47), the instanton contribution to the action [Eq. (45)] is $S_k = k\mathbf{b}_\perp^2/2\chi\alpha'$, leading to the announced factor of e^{-S_k} in Eq. (26).

V. SCHWINGER-UNRUH CONNECTION

The instanton world-sheet solution [Eq. (47)] has a simple kinematical interpretation. Indeed, since Eq. (46) refers to a "magnetic field" along the transverse 01 direction, Eq. (47) describes a "cyclotron" motion of the string instanton in the 01 plane with cyclotron frequency $\omega_k = 2\pi k/T$. In Minkowski signature, the motion is hyperbolic with local acceleration

$$a(\sigma) = \frac{1}{R(\sigma)} = \frac{\chi}{\mathbf{b}_\perp}\frac{1}{\cosh(\chi(\sigma - 1/2))}. \tag{48}$$

The acceleration is maximum at the center of the string, $\sigma = 1/2$. Due to this local acceleration, the string feels a σ-dependent Unruh temperature

$$T_U(\sigma) = \frac{a(\sigma)}{2\pi}$$

that is maximal at the center with $T_U = \chi/2\pi\mathbf{b}_\perp \equiv 1/\beta$. This interpretation has a deeper physical meaning—note that the line element associated with the instanton [Eq. (47)] in Minkowski signature is

$$ds^2 \approx -a^2R^2 d(\tau\mathbf{b}_\perp)^2 + dR^2 + dx^{\perp 2}. \tag{49}$$

Equation (49) refers to a Rindler line element with Rindler time $t(\tau) = \tau\mathbf{b}_\perp$. The Rindler acceleration $a = \chi/\mathbf{b}_\perp$ implies a Rindler horizon $\mathbf{R} = 1/2a$ at the position of the instanton which is the tip of the light cone in our dipole-dipole scattering setup.

The occurrence of the world-sheet instanton is analogous to the formation of a dynamic black hole at the tip of the light cone. Although this five-dimensional black hole extends in the conformal direction, it is very different from the standard black hole widely used in holographic equilibrium. It is similar to the four-dimensional black hole suggested in Ref. [39] using arguments based on saturation and a reinterpretation of the standard Schwinger particle pair-creation process [40]. To contrast our analysis with that of Ref. [39], we will briefly review the arguments in the latter. Starting from the Schwinger pair-production rate in a longitudinal electric field in scalar QED, the Unruh temperature is identified as

$$e^{-\frac{\pi m^2}{eE}} \equiv e^{-\frac{\pi m}{a}} \equiv e^{-\frac{m/2}{T_U}}, \tag{50}$$

with $T_U = a/2\pi = eE/2\pi m$. In Ref. [39], this QED result was exported to the QCD color glass through the identification of $eE/m \to \mathbf{Q}_S$, the QCD saturation scale. This argument is different from ours in a number of ways: 1) Our induced electric field $E \approx \sigma_T\chi$ is kinematical and longitudinal as opposed to $eE \approx \mathbf{Q}_S^2$, which is dynamic and transverse. 2) The scale is set by the string length (strong coupling) and not the saturation length (weak coupling). 3) Our Unruh temperature follows from a stringy pair-creation process, not a particle pair-creation process. 4) Our strings are holographic in hyperbolic space to account for the conformal nature of QCD in the ultraviolet. 5) Our black hole forms at the tip of the light cone but extends in the holographic or fifth direction.

VI. ENTROPY

As we detailed in Sec. IV, the stringy instanton solution [Eq. (47)] reduces the on-shell action [Eq. (45)] to

$$S_k \approx \frac{1}{2}\sigma_k \mathbf{b}_\perp \beta, \tag{51}$$

with the k-string tension $\sigma_k = k\sigma_T$ for N-ality k. For QCD with three colors, only the N-alities $k = 1, 2$ are allowed [41]. For QCD at large N_c, all N-alities up to the integer value of $N_c/2$ are allowed. Only the N-ality $k = 1$ is selected in the process of scattering dipoles in the fundamental representation. We argue below that $k = 2$ is released in *dense AA* collisions.

Equation (51) receives quantum contributions in the form of world-sheet fluctuations (Luscher term), that translates to Gribov diffusion at strong coupling. For large χ and $\mathbf{b}_\perp$, the quantum [$\mathcal{O}(n)$] and curvature [$\mathcal{O}(1/\sqrt{\lambda})$] corrections are readily implemented by the diffusive nature of the propagator as reviewed in Sec. III. The dominant quantum correction follows from the transverse diffusion of the tachyonic mode ($n = 0$) in $\mathrm{AdS}_{D_\perp}$. To order $1/\sqrt{\lambda}$, we obtain

$$S_k \approx \frac{1}{2}\sigma_k \beta \mathbf{b}_\perp - \frac{2\pi \mathbf{b}_\perp}{\beta}\left(\frac{D_\perp}{12k} - \frac{(D_\perp - 1)^2}{8\sqrt{\lambda}}\right). \tag{52}$$

This Euclidean stringy action amounts to a free energy $F_k = S_k/\beta$, where the temperature is the Unruh temperature $1/\beta$ on the string. In the collision process this entropy is deposited over a short time, as we detail below. It follows that Eq. (52) carries an entropy

$$\mathbf{S}_k \equiv \beta^2 \frac{\partial F_k}{\partial \beta} \approx \chi\left(\frac{D_\perp}{6k} - \frac{(D_\perp - 1)^2}{4\sqrt{\lambda}}\right), \tag{53}$$

or equivalently,

$$\mathbf{S}_k \approx 2(\alpha_{\mathbf{P}k} - 1)\chi. \tag{54}$$

For $k = 1$, the Pomeron intercept is $(\alpha_{\mathbf{P}1} - 1) \approx 0.15$, and the entropy per unit rapidity is about $1/3$. Using the optical theorem, the virtual wee-dipoles become on shell, and their contribution to the entropy gives

$$\mathbf{S}_k \approx \ln N^2_{\mathrm{wee},k}, \tag{55}$$

where $N_{\mathrm{wee},k}$ is the total number of wee-dipoles surrounding each of the incoming dipole pairs involved in the collision

$$N_{\mathrm{wee},k} = \int dud\mathbf{b}_\perp \mathbf{N}_\mathbf{k} = e^{(\alpha_{\mathbf{P}k}-1)\chi}. \tag{56}$$

This is to be contrasted with the fully thermal or incoherent expectation of $\ln N$ and the fully Poissonian or coherent expectation of $\ln\sqrt{N}$, with N the mean multiplicity number.

Most of this entropy is the result of the tachyon excitation on the string. Indeed, for a large impact parameter $\mathbf{b}_\perp$, the Unruh temperature is smaller than the Hagedorn temperature,

$$T_U = \frac{\chi}{2\pi \mathbf{b}_\perp} < T_H = \sqrt{\frac{3\sigma_T}{\pi D_\perp}}, \tag{57}$$

which translates to $\mathbf{b}_\perp > \chi/(2\pi T_H)$. As the impact parameter is reduced, the Unruh temperature increases, causing the string excitations to exponentiate, leading to a Hagedorn transition. At the Hagedorn point, it may be mapped on the Bekenstein-Hawkins (BH) temperature of a microscopic black hole [42–45].

VII. FORMATION TIME

Over what time is the entropy [Eqs. (54) and (55)] associated with the dipole-dipole collision released? To answer this question, we note that the emergence of an Unruh temperature on the string world sheet suggests that semiclassically the metric is locally Rindler; see Eq. (49).

We now argue that the prompt release time t_R can be set to be the time when the diffusing string in transverse $\mathrm{AdS}_{D_\perp}$ reaches the effective size of the Rindler horizon $\mathbf{R}$ by analogy with the time it takes to a string to fall on a black hole [43,46]. Indeed, the string diffusion in rapidity causes the transverse string size to increase as

$$\langle x_\perp^2 \rangle = \chi\alpha' \equiv \mathbf{D}_R t(1), \tag{58}$$

with the diffusion constant in Rindler space, $\mathbf{D}_R = \alpha'/(2\mathbf{R})$. Through the last equality, we reinterpret Eq. (58) as a diffusion in Rindler space over a typical Rindler time $t(1) = \mathbf{b}_\perp$. The release entropy time t_R is then set by the condition $\mathbf{R}^2 = \mathbf{D}_R t_R$, or

$$t_R = 2\frac{\mathbf{R}^3}{\alpha'} = 2\frac{(\mathbf{b}_\perp/2\chi)^3}{\alpha'}. \tag{59}$$

For a QCD string with $\alpha' = 1/(2\ \mathrm{GeV})^2 = (0.1\ \mathrm{fm})^2$ and a typical impact parameter $\mathbf{b}_\perp \sim 10\sqrt{\alpha'}$, this results in $t_R \sim (25\ \mathrm{fm})/\chi^3$, which is short.

VIII. pp MULTIPLICITIES

pp collisions at large rapidity χ can be viewed as dipole-dipole scattering from each colliding proton [28]. The density of dipoles in the proton is set by the saturation momentum $\mathbf{Q}_S \equiv \sqrt{2}/z_S$. In holographic QCD, this follows from the transcendental equation [17]

$$\frac{z_S}{\sqrt{2}}\mathbf{Q}_S(\chi, \mathbf{b}_\perp) = \frac{g_s^2}{2}(2\pi\alpha')^{3/2} z_S z_p \mathbf{N}(\chi, z_S, z_p, \mathbf{b}_\perp) = 1, \tag{60}$$

with the effective string coupling g_s and typical proton virtuality $1/z_p$. Unlike in a partonic model, the colorless wee-dipoles are the objects that saturate the transverse density.

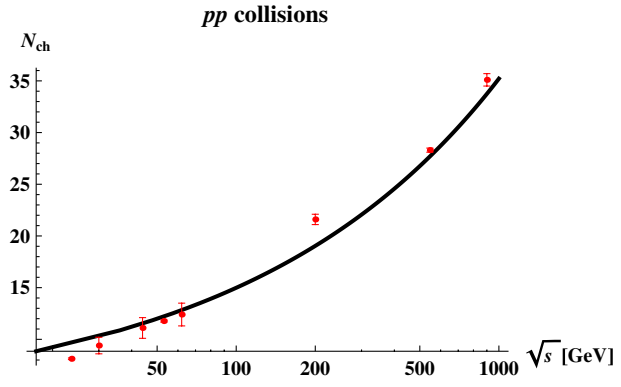

FIG. 3 (color online). Energy dependence of the charged multiplicity for pp collisions; see text.

In solving for $\mathbf{Q}_S$ in Eq. (60), all the holographic parameters are set by the DIS data analysis in Refs. [17,28]: $\lambda = 23$, $D_\perp = 3$, $g_s = 1.5$, $z_p = 1.8\,\mathrm{GeV}^{-1}$, $z_0 = 2\ \mathrm{GeV}^{-1}$, $s_0 = 10^{-2}\ \mathrm{GeV}^2$. If $A_{pp} \approx 1\ \mathrm{fm}^2$ is the typical proton area, then $A_{pp}\mathbf{Q}_S^2 \approx 12$ is the typical number of dipoles with $\mathbf{Q}_S^2 \approx 1/2\ \mathrm{GeV}^2$ the typical squared saturation momentum. Thus, for pp collisions, the typical entropy release per unit of rapidity is

$$\mathbf{S}_{pp}/\chi \approx (A_{pp}\mathbf{Q}_S^2) \times (\mathbf{S}_1/\chi) \approx 12 \times \frac{1}{3} = 4. \quad (61)$$

In holography, the scaling of the entropy with the energy follows from the scaling of the saturation momentum [Eq. (60)] with rapidity. In the conformal limit and at large χ, the entropy asymptotes

$$\mathbf{S}_{pp} \approx \left(\frac{s}{s_0}\right)^{\left(\sqrt{1+2\sqrt{\lambda}(\alpha_{\mathbf{P}}-1)}-1\right)\Big/\sqrt{\lambda}} \ln(s/s_0), \quad (62)$$

which is $\mathbf{S}_{pp} \approx (s/s_0)^{0.228} \ln(s/s_0)$ using the parameters set by the DIS data. In Fig. 3, we show the pp charged multiplicities [5]

$$N_{ch,pp} = \mathbf{S}_{pp}/7.5 \quad (63)$$

at collider energies [47], with $\mathbf{b}_\perp = 1/3$ fm. A recent discussion of the entropy in the context of saturation models was made in Ref. [48].

IX. pA, AA MULTIPLICITIES

We note that for pA collisions, $A_{pA} \approx A^{1/3}A_{pp}$, so that $\mathbf{S}_{pA}/\mathbf{S}_{pp} \approx A^{1/3}$. In AA collisions, if the collision is mainly between dipoles with N-ality $k = 1$, a similar scaling with the nucleus number $A = A^{1/3} \times A^{2/3}$ is expected to take place. Here $A^{1/3}$ Lorentz contracted nucleons can be distributed in the $A^{2/3}$ transverse nucleus size. However, when the nucleons start to overlap, the $k = 2$ N-ality can be exchanged:

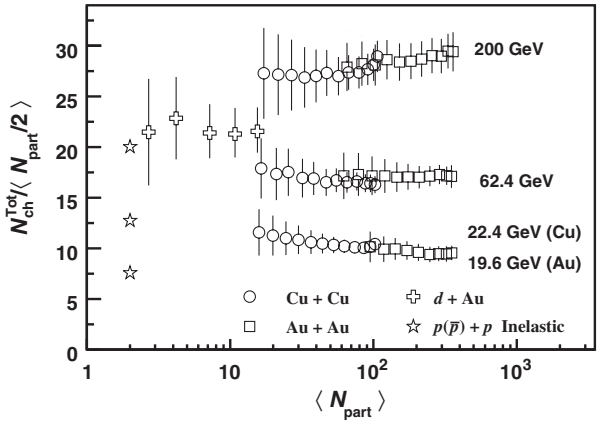

FIG. 4. Scaling of the total charged multiplicities with the number of participants [49]; see text.

$$\frac{\mathbf{S}_{AA}}{\mathbf{S}_{pp}} \approx A\left(\sum_1^{[N_c/2]} \frac{1}{k}\right). \quad (64)$$

In QCD with $N_c = 3$, the sum is $3/2$. The contribution of the $k = 2$ N-ality is expected to take place when the number of participants is about ten, so that $10^{1/3} \approx 2$ corresponds to two overlapping nucleons.

In Fig. 4, we show the total charged multiplicities normalized to the averaged number of participants as a function of the number of participants for a range of collider energies [49]. For a fixed collider energy, we note the characteristic $3/2$ jump from pp to AA collisions at a number of participants of around ten.

The charged multiplicity follows as $N_{ch,\mathrm{AuAu}} = 3/2\langle \mathrm{Au}\rangle \mathbf{S}_{pp}/7.5$, with the average participating gold nucleon number $\langle \mathrm{Au}\rangle$. Using the same numerical values as for $N_{ch,pp}$ and $\langle \mathrm{Au}\rangle = 175$ for most central collisions [50], Fig. 5 shows an agreement of our holographic result with the experimental data at high energies, where the inelasticities are large. At LHC energies, we expect $N_{ch,pp} \sim 54$, $N_{ch,p\mathrm{Pb}} \sim 320$, $N_{ch,\mathrm{PbPb}} \sim 16800$ at $\sqrt{s} = 2.76$ TeV and $N_{ch,pp} \sim 82$, $N_{ch,p\mathrm{Pb}} \sim 470$, $N_{ch,\mathrm{PbPb}} \sim 23400$ at $\sqrt{s} = 7$ TeV using $\langle A_{\mathrm{PbPb}}\rangle = 191$ [51].

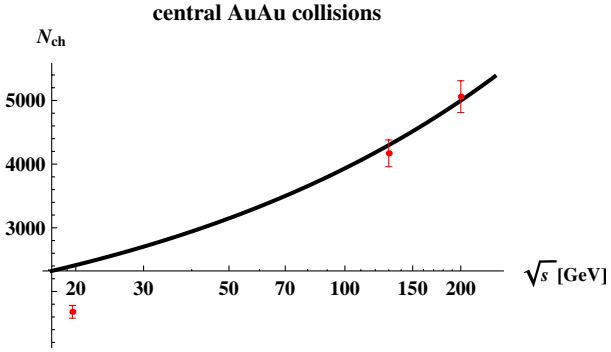

FIG. 5 (color online). Energy dependence of the charged multiplicity for central AuAu collisions. See text.

X. CONCLUSIONS

We have suggested that the Pomeron viewed as an exchange of an instanton on the string world sheet carries a free energy $F_k/T_U = S_k$, with S_k the instanton action of N-ality k and T_U the Unruh temperature. For a large impact parameter $\mathbf{b}_\perp$, the Unruh temperature is low, and the entropy is mostly carried by the lowest string excitation, which is tachyonic. This stringy entropy is neither coherent nor thermal.

For smaller impact parameters, the Unruh temperature may reach the Hagedorn temperature, transmuting the stringy entropy to partonic entropy. The latter is likely commensurate with the Bekenstein-Hawkins entropy, and the onset of a microscopic black hole. Macroscopic black holes [4–8] may be aggregates of these coalescing microscopic black holes, as suggested initially in Ref. [4] and more recently in Ref. [52].

We have argued that typical pp, pA and AA collisions at current collider energies may probe this stringy entropy with low Unruh temperature. At large rapidities, the holographic entropy is in agreement with the data for the energy scaling of the charged multiplicities. The $3/2$ jump in the charged multiplicities reported by the current collider experiments with a number of participants of ten or higher is explained by the exchange of N-ality $k = 1, 2$ strings. We expect similar jumps in the transport parameters, e.g. viscosity and flow.

Although the measured total multiplicities reflect on the final state hadronic produces, entropy conservation guarantees that our prompt and initial entropy estimates are lower bounds. The general lore of energy and momentum conservation, say through viscous hydrodynamics evolution, suggests only a moderate increase of the total entropy by about 25% in going from initial to final states, making our estimates plausible.

ACKNOWLEDGMENTS

We would like to thank Gokce Basar, Dima Kharzeev and Edward Shuryak for discussions. This work was supported by the U.S. Department of Energy under Contract No. DE-FG-88ER40388.

[1] D. Kharzeev, E. Levin, and M. Nardi, Phys. Rev. C **71**, 054903 (2005); Nucl. Phys. **A747**, 609 (2005); B. Schenke, P. Tribedy, and R. Venugopalan, Phys. Rev. C **86**, 034908 (2012).
[2] R. Baier, A. H. Mueller, D. Schiff, and D. T. Son, Phys. Lett. B **539**, 46 (2002); arXiv:1103.1259.
[3] R. J. Fries, B. Muller, and A. Schafer, Phys. Rev. C **79**, 034904 (2009).
[4] E. Shuryak, S.-J. Sin, and I. Zahed, J. Korean Phys. Soc. **50**, 384 (2007).
[5] S. S. Gubser, S. S. Pufu, and A. Yarom, Phys. Rev. D **78**, 066014 (2008).
[6] S. Lin and E. Shuryak, Phys. Rev. D **79**, 124015 (2009).
[7] B. Wu and P. Romatschke, Int. J. Mod. Phys. C **22**, 1317 (2011).
[8] E. Kiritsis and A. Taliotis, J. High Energy Phys. 04 (2012) 065.
[9] A. Donnachie and P. V. Landshoff, Phys. Lett. B **296**, 227 (1992).
[10] V. N. Gribov, in *Gauge Theories and Quark Confinement* (Phasis, Moscow, 2002).
[11] E. A. Kuraev, L. N. Lipatov, and V. S. Fadin, Zh. Eksp. Teor. Fiz. **72**, 377 (1977) [Sov. Phys. JETP **45**, 199 (1977)].
[12] G. Basar, D. E. Kharzeev, H.-U. Yee, and I. Zahed, Phys. Rev. D **85**, 105005 (2012).
[13] M. Rho, S.-J. Sin, and I. Zahed, Phys. Lett. B **466**, 199 (1999).
[14] R. A. Janik and R. B. Peschanski, Nucl. Phys. **B565**, 193 (2000); **B625**, 279 (2002).
[15] R. C. Brower, J. Polchinski, M. J. Strassler, and C.-I. Tan, J. High Energy Phys. 12 (2007) 005; R. C. Brower, M. J. Strassler, and C.-I. Tan, J. High Energy Phys. 03 (2009) 092.
[16] P. Castorina, D. Kharzeev, and H. Satz, Eur. Phys. J. C **52**, 187 (2007).
[17] A. Stoffers and I. Zahed, Phys. Rev. D **87**, 075023 (2013).
[18] O. Nachtmann, Ann. Phys. (N.Y.) **209**, 436 (1991).
[19] O. Nachtmann, in *Lectures on QCD*, edited by F. Lenz (Springer-Verlag, Berlin, 1997), pp. 1–86.
[20] G. P. Korchemsky, Phys. Lett. B **325**, 459 (1994).
[21] A. I. Shoshi, F. D. Steffen, and H. J. Pirner, Nucl. Phys. **A709**, 131 (2002).
[22] A. Kramer and H. G. Dosch, Phys. Lett. B **252**, 669 (1990).
[23] H. G. Dosch, E. Ferreira, and A. Kramer, Phys. Rev. D **50**, 1992 (1994).
[24] D. E. Berenstein, R. Corrado, W. Fischler, and J. M. Maldacena, Phys. Rev. D **59**, 105023 (1999).
[25] D. J. Gross and H. Ooguri, Phys. Rev. D **58**, 106002 (1998).
[26] K. Zarembo, Phys. Lett. B **459**, 527 (1999).
[27] J. Sonnenschein and A. Loewy, J. High Energy Phys. 01 (2000) 042.
[28] A. Stoffers and I. Zahed, arXiv:1210.3724.
[29] J. Polchinski and M. J. Strassler, Phys. Rev. Lett. **88**, 031601 (2002).
[30] G. Veneziano, Nucl. Phys. **B117**, 519 (1976).
[31] E. Meggiolaro, Z. Phys. C **76**, 523 (1997).
[32] E. Meggiolaro, Eur. Phys. J. C **4**, 101 (1998).
[33] S. J. Brodsky, Eur. Phys. J. A **31**, 638 (2007).
[34] S. Fubini, D. Gordon, and G. Veneziano, Phys. Lett. **29B**, 679 (1969).

[35] V. N. Gribov, in *Proceedings of the 8th LNPI Winter School on Nuclear and Elementary Particle Physics* (1973), p. 5; V. N. Gribov, in *Gauge Theories and Quark Confinement* (Phasis, Moscow, 2002), p. 3.
[36] V. N. Gribov and L. N. Lipatov, Yad. Fiz. **15**, 781 (1972) [Sov. J. Nucl. Phys. **15**, 438 (1972)].
[37] J. Greensite, Nucl. Phys. **B249**, 263 (1985).
[38] C. Schubert, J. Phys. Conf. Ser. **287**, 012031 (2011).
[39] D. Kharzeev and K. Tuchin, Nucl. Phys. **A753**, 316 (2005).
[40] J. S. Schwinger, Phys. Rev. **82**, 664 (1951).
[41] J. Greensite, Prog. Part. Nucl. Phys. **51**, 1 (2003).
[42] A. Strominger and C. Vafa, Phys. Lett. B **379**, 99 (1996).
[43] L. Susskind, in *The Black Hole*, edited by C. Teitelboim (World Scientific, Singapore, 1998), pp. 118–131.
[44] G. T. Horowitz and J. Polchinski, Phys. Rev. D **55**, 6189 (1997).
[45] R. R. Khuri, Nucl. Phys. **B588**, 253 (2000).
[46] L. Susskind, Phys. Rev. D **49**, 6606 (1994).
[47] M. Basile *et al.*, Nuovo Cimento A **65**, 400 (1981); W. Thome *et al.* (Aachen-CERN-Heidelberg-Munich Collaboration), Nucl. Phys. **B129**, 365 (1977); G. J. Alner *et al.* (UA5 Collaboration), Phys. Lett. **167B**, 476 (1986).
[48] K. Kutak, Phys. Lett. B **705**, 217 (2011).
[49] B. Alver *et al.*, Phys. Rev. Lett. **102**, 142301 (2009).
[50] B. B. Back *et al.*, Phys. Rev. Lett. **91**, 052303 (2003).
[51] K. Aamodt *et al.* (ALICE Collaboration), Phys. Rev. Lett. **106**, 032301 (2011).
[52] E. Shuryak and I. Zahed, arXiv:1301.4470.